LIMNOLOGY and OCEANOGRAPHY LETTERS

ASLO

Open Access

Limnology and Oceanography Letters 11, 2026, e70096

doi: 10.1002/lol2.70096

LETTER

Field measurements and model predictions of turbulent kinetic energy in canopies of sparse vegetation under tidal flows

Vinay Nelli [1]* **Julia C. Mullarney** [1] **Rémi Chassagne** [1,2] **William Nardin** [3] **Rafael O. Tinoco** [4]

[1]Coastal Marine Group, School of Science, University of Waikato, Hamilton, New Zealand; [2]Université Grenoble Alpes, LEGI, CNRS UMR 5519, Grenoble, France; [3]University of Maryland Center for Environmental Science, Cambridge, Maryland, USA; [4]Department of Civil and Environmental Engineering, University of Illinois, Urbana-Champaign — UIUC, Champaign, Illinois, USA

Scientific Significance Statement

Aquatic vegetation such as mangroves can act as a nature-based solution to reduce coastal erosion and mitigate the effects of sea-level rise. A recent new paradigm has suggested that turbulent kinetic energy is the critical parameter controlling sediment movements in these environments. Yet, models to predict this variable have been developed based on highly simplified laboratory experiments. We present field observations from natural subtropical mangroves to test the laboratory-derived models in a real and heterogeneous system, characterized by multiple vegetation length scales. Crucially, the model only worked well if predictions incorporated the largest length scales, underscoring the need to account for the wider environmental setting. The results likely also showcase a different flow regime to the denser canopies more commonly found in tropical mangrove environments.

Abstract

The presence of vegetation in aquatic environments alters hydrodynamics and sediment resuspension. A recent paradigm has suggested that turbulent kinetic energy (TKE) serves as a better predictor of sediment transport in aquatic canopies than bed shear stress. This observation has led to the development of formulations to predict TKE for vegetated flows in the laboratory. However, model validation from natural heterogeneous field environments is lacking. Here, we explore the application of laboratory-based formulas in a real environment, characterized by multiple vegetation length scales. We measured turbulence within a sparse canopy of mangrove pneumatophores and saplings during an experimental period with negligible wind-wave activity. The existing formulations for TKE performed well in the field, but only when using the measured values for horizontal eddy length scales. These length scales accounted for the generation of additional turbulence from the surrounding sapling canopy, leading to notably larger TKE values than in similar laboratory experiments.

Aquatic vegetation provides habitat for different species (Costanza et al. 1997; van Katwijk et al. 2016), stabilizes riverbanks (Barbier et al. 2011; Pollen and Simon 2005) and attenuates waves and storm surges in coastal regions (Vettori et al. 2025; Temmerman et al. 2023; Montgomery et al. 2019; Hu et al. 2025). The effectiveness of aquatic vegetation in

*Correspondence: sn262@students.waikato.ac.nz

Associate editor: Nathan Hall

mitigating coastal hazards has led to the use of some species being promoted as a soft engineering solution against coastal erosion. However, at present, accurate and long-term predictions of the efficacy of such approaches are limited, as the processes controlling the movement and resuspension of sediment in these environments are still not fully constrained (Nepf 2012b, 2012a). Studies of sediment transport in regions with aquatic vegetation have shown that the presence of vegetation significantly alters the near-bed flow (Yager and Schmeeckle 2013; Yang et al. 2015; Conde-Frias et al. 2023). Moreover, a recent shift in the sediment transport paradigm argues that traditional approaches for bare-bed flows based on shear stress predictors are inaccurate for vegetated environments, and that turbulent kinetic energy (TKE) is a better predictor of sediment motion (Yang et al. 2016; Tinoco and Coco 2018).

While recent laboratory (Yang et al. 2015; Chen et al. 2020; M. Liu, Huai, et al. 2021) and numerical (Etminan et al. 2018; Anjum and Tanaka 2020; King et al. 2012) studies have shown that TKE can be accurately predicted in vegetated channels, these works use a myriad of simplifications which induce bias in the results (Tinoco et al. 2020). Horstman et al. (2018) conducted laboratory experiments with smooth cylindrical dowels and real vegetation, and concluded that dowels poorly mimic pneumatophores. Field studies in natural environments with complex non-stationary hydrodynamics, varying submergence levels, asymmetric tidal flow, and heterogeneous vegetation remain rare. Recent data from mangrove canopies show the direct dependence of bed-level changes on TKE and a positive relationship between TKE intensity and vegetation density (Norris et al. 2019, 2021); emphasizing the need for an accurate TKE prediction model, which is applicable to complex natural environments.

Here, we report high-resolution (temporal and spatial) field measurements of velocity and turbulence within a sparse canopy of *Avicennia marina* mangrove roots. The measurements of TKE are then compared to predictions from laboratory-derived models over changing water depths and velocities observed during a tidal period.

Models to predict TKE in pneumatophore canopies

The TKE in vegetated aquatic environments is commonly approximated as the sum of two independent terms: a bed-generated, and a vegetation-generated component. This section will provide insights into the formulation of the contributions and introduce the combined TKE formulation.

Bed shear stress in open channels is related to the mean flow speed as $\tau = \rho C_f U^2$ (Schlichting 1979; Williams 1995), in which τ is the bed shear stress, U is the depth-averaged flow speed, ρ is the density of water, and C_f is the bed friction factor. The shear stress equation can then be recast in terms of TKE using the relation $k_{bed} = \tau/(0.19\rho)$ (Soulsby 1983), yielding an expression for bed-generated TKE as

$$k_{bed} = \frac{C_f}{0.19} U^2 \tag{1}$$

Vegetation-generated TKE (k_{veg}), produced at the scale of the root diameter, can be estimated assuming a local balance between turbulence production in stem wakes and viscous dissipation as (Tanino and Nepf 2008),

$$k_{veg} = \delta \left(C_D \frac{\phi}{(1-\phi)\pi/2} \frac{l_t}{d} \right)^{2/3} U^2 \tag{2}$$

in which C_D is the form drag coefficient for individual stems, $\phi = n\pi d^2/4$ is the solid volume fraction for arrays of cylindrical elements, n is the number of stems per m^2, d is the stem diameter, l_t is the characteristic eddy length-scale, and δ is an empirical scale coefficient. Large eddy simulations (Etminan et al. 2018) have been conducted for various staggered arrays of vegetation, revealing that form drag can be accurately predicted as

$$C_D = 0.9\zeta^2 \left[1 + 10 \left(\frac{\zeta U d}{\nu} \right)^{-2/3} \right] \tag{3}$$

in which ν is the kinematic viscosity of water, and the coefficient $\zeta = \frac{1-\phi}{1-\sqrt{2\phi/\pi}}$ is the ratio of average velocity in the smallest cross-section (maximum constriction) to the mean velocity of the flow. Combining Expressions 1 and 2 for bed- and vegetation-generated turbulence, we obtain the present model for predicting total TKE, k_t^{pred}, in pneumatophore canopies

$$k_t^{pred} = \begin{cases} \underbrace{\frac{C_f}{0.19} U^2}_{k_{bed}} + \underbrace{\delta \left[\left(C_D \frac{\phi}{(1-\phi)\pi/2} \frac{l_t}{d} \right)^{2/3} U^2 \right]}_{k_{veg}}, & \text{Near-bed} \\ \underbrace{\delta \left[\left(C_D \frac{\phi}{(1-\phi)\pi/2} \frac{l_t}{d} \right)^{2/3} U^2 \right]}_{k_{veg}}, & \text{In the canopy} \end{cases} \tag{4}$$

The distinction between near-bed and in-canopy TKE is defined later in the manuscript within the context of this study. This TKE formulation has been recently validated by many laboratory experiments (Yang and Nepf 2018; Zhao and Nepf 2021; C. Liu, Shan, et al. 2021, among others), and large eddy simulations (Etminan et al. 2018). In the present work, we test this formulation with field observations.

Field site and instrumentation

The data presented in this study were collected in Purangi estuary, New Zealand (−36.84°N, 175.76°E) over six full tidal cycles from 08 September 2022 to 12 September 2022.

Measurements were taken inside and around a small stand of *Avicennia marina* mangroves (Fig. 1). At the measurement location (red square in Fig. 1), the vegetation consisted primarily of pneumatophore roots and sparsely populated juvenile mangroves ("saplings") of average cross-sectional span of ≈0.1 m diameter, ≈0.2 m height with leaves, and a density of 3–5 saplings per m^2. Adjacent to the site was a line of medium-size mangrove trees of an average cross-sectional span of 1–2 m diameter, and 1–1.5 m height (green ellipse, Fig. 1B). The flood and ebb flow directions were aligned with the orientation of the mangrove trees (Supporting Information Fig. S1) and speeds were slow enough to assume that the mangrove trees have no effect on the study site. The pneumatophores and saplings did not move under the currents and thus can be

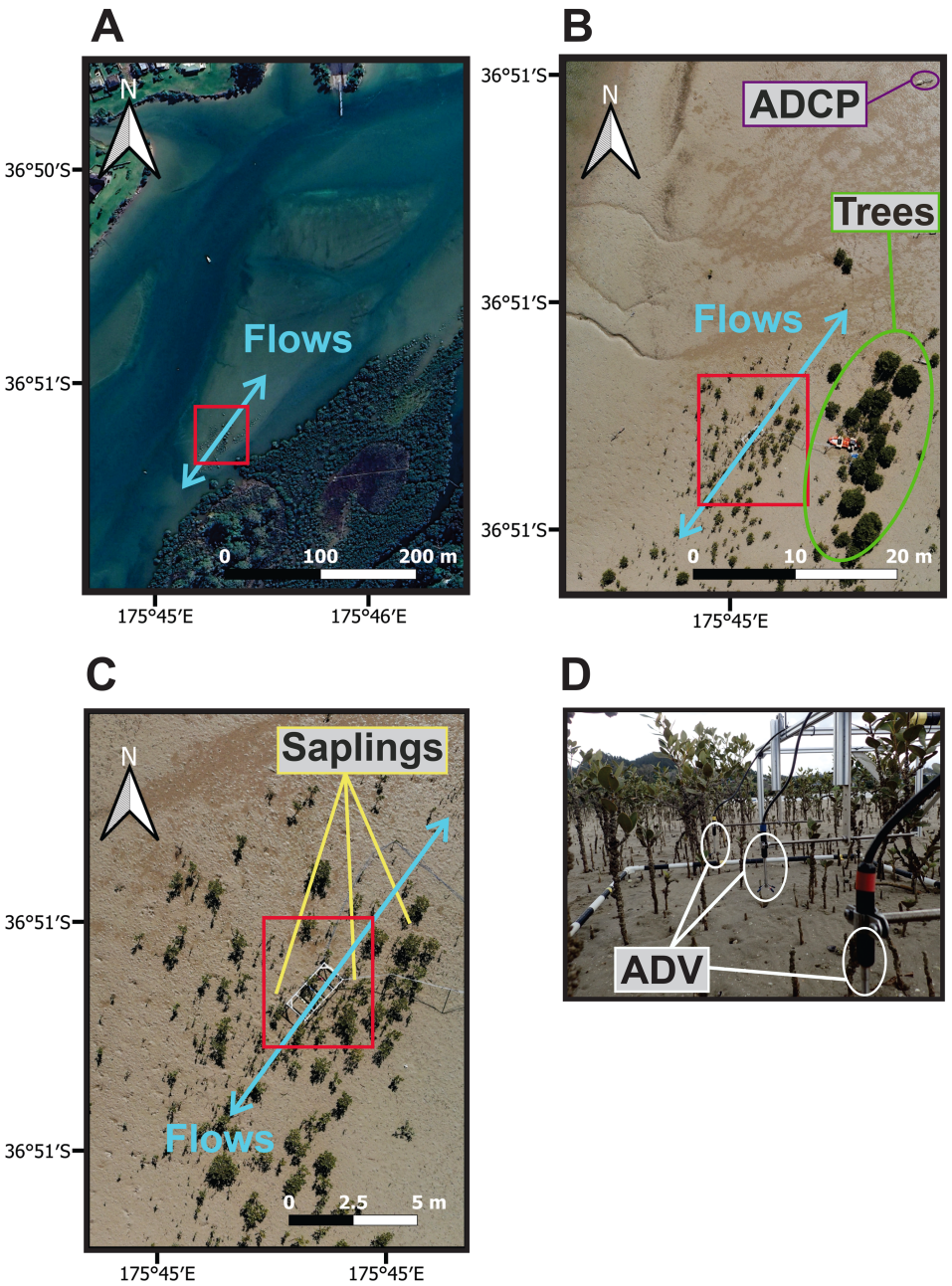

Fig. 1. Field deployment. (**A**) Satellite image of the Purangi Estuary with the field site shown in the red square, and principal flow axis shown in blue. (**B**) Geo-rectified drone image of the field site showing the locations of the profiling ADVs (red square), ADCP (purple circle), and mangrove trees (green). (**C**) Geo-rectified close-up drone image of the field site showing the locations of the profiling ADVs (red square), and example mangrove saplings (yellow). (**D**) Photograph of the Vectrino Profilers (white circle), and surrounding sapling canopy (plants with leaves).

treated as rigid vegetation. Furthermore, the frontal area density at the site ($ah < 0.035$) was low enough to assume canopy-scale shear layer vortices were not generated.

Near-bed velocities and pressure over bare-bed (purple circle, Fig. 1B) were measured by a downwards-looking Acoustic Doppler Current Profiler (ADCP, 2 MHz Nortek Aquadopp) operating in pulse-coherent mode. The instrument was positioned 0.21 m above the bed and collected data at a rate of 8 Hz, with 25 mm vertical resolution and a blanking distance of 54 mm. A conductivity–temperature–depth sensor (RBR Concerto) was positioned inside the pneumatophore canopy to measure local water depth, temperature, and salinity.

Three profiling Acoustic Doppler Velocimeters (ADVs—10 MHz Nortek Vectrino Profilers) were deployed to measure flow velocities within and above the sparse pneumatophore canopy. The ADVs recorded three components of velocity over a vertical profile of 30 mm with 1-mm spatial resolution at a rate of 50 Hz. The center ADV was positioned to capture flows close to the bed (0–30 mm height above bed) for the full duration of the experiment, while the other two ADVs were moved in between tides in both horizontal and vertical directions to capture measurements at three different heights above the bed (0–30, 70–100, and 96–126 mm) and two horizontal positions. Instrument positions are summarized in Supporting Information Table S1.

Sediment grain size was determined from surface grab samples using a particle size Analyzer (Malvern Mastersizer 3000). Pneumatophores characteristics were estimated in 1-m^2 quadrats placed below the ADVs using structure-from-motion techniques and the sector-slice algorithm of Liénard et al. (2016), applied to over 100 images. This analysis provided estimates of the pneumatophore parameters, stem diameter (d), number of stems per square meter (n), frontal area density $a = nd$, and solid volume fraction $\phi = \pi nd^2/4$ as a function of height above the bed.

Data quality control and processing

The data from the ADCP over the duration of experiments (six tides) were used to determine the bare-bed friction factor $C_f = \tau/(\rho U^2)$ using the open channel flow approximation (Schlichting 1979), and observed bed shear stress $\tau = C_2 0.5 \rho w'^2$, where $C_2 = 0.9$, and w' are the turbulent velocity fluctuations in the vertical direction (Biron et al. 2004; Kim et al. 2000). The ADCP was downward-looking at 210 mm from bed level. The velocity fluctuations used in estimation of C_f are from the bin closest to the bed level at 31 mm, close to the suggested measurement height of 0.1 of water depth by (Biron et al. 2004) for estimating shear stress from turbulence measurements.

Low-quality velocity data from the ADVs (correlations < 70%, and SNR < 10 dB) were removed, with gaps filled by linear interpolation. Velocities from cells from below the identified bed level were removed. The tidal flow was observed to have a principal axis with mean flow direction (to) during flood of 250° and 50° during the ebb (Supporting Information Fig. S1). Therefore, velocities were rotated with positive u into the flood direction (250°SW), v perpendicular to the flood direction (340°), and w is the vertical velocity (positive upwards). Finally, the data were despiked using the phase-space thresholding method (Goring and Nikora 2002).

For each instrument, TKE was calculated over 3-min windows with a 1.5-min overlap:

$$k_t^{(\mathrm{meas})} = \left\langle \overline{(u'^2 + v'^2 + w'^2)/2} \right\rangle \tag{5}$$

in which u', v', and w' are the fluctuations from the mean over each window, the overbar represents a temporal average and the angle brackets denote an average over all vertical bins.

In Eqs. 1 and 2, the two contributions of the total TKE were modeled based on the depth-averaged (channel-averaged) velocity. In our experiments we have used the velocity averaged over the short (30 mm) ADV profile, noting (Xu and Nepf 2020) measured TKE in two canopies made with real plant morphologies and found similar results when using either depth-averaged velocities, or velocities averaged over the canopy height.

The observed bed-generated turbulence $k_{\mathrm{bed}}^{(\mathrm{estim})}$ was estimated using the mean horizontal speed $U = \left\langle \overline{\sqrt{u^2 + v^2}} \right\rangle$ in Eq. 1. The vegetation-generated turbulence was then estimated as,

$$k_{\mathrm{veg}}^{(\mathrm{meas})} = \begin{cases} k_t^{(\mathrm{meas})} - k_{\mathrm{bed}}^{(\mathrm{estim})}, & \text{Profiler at bed} \\ k_t^{(\mathrm{meas})}, & \text{Profiler away from bed} \end{cases} \tag{6}$$

The ADVs were moved between three different heights above bed with the closest profile to bed in the range of 0–30 mm. Therefore, we define measurement heights below 30 mm as close to the bed. The parameter δ required for predicting vegetation-generated TKE k_{veg} (Eq. 2) is then computed by fitting against the observed vegetation-generated TKE, that is,

$$\delta = \begin{cases} \dfrac{k_t^{(\mathrm{meas})} - k_{\mathrm{bed}}^{(\mathrm{estim})}}{\left(C_{\mathrm{D}} \frac{\phi}{(1-\phi)\pi/2} \frac{l_t}{d}\right)^{2/3} U^2}, & \text{Profiler at bed} \\ \dfrac{k_t^{(\mathrm{meas})}}{\left(C_{\mathrm{D}} \frac{\phi}{(1-\phi)\pi/2} \frac{l_t}{d}\right)^{2/3} U^2}, & \text{Profiler away from bed} \end{cases} \tag{7}$$

The errors in prediction were estimated using mean absolute percentage error (MAPE) defined as

$$\mathrm{MAPE} = \sum \left(100 \times \left| \left(k_t^{(\mathrm{meas})} - k_t \right) \right| / k_t^{(\mathrm{meas})} \right) / N \tag{8}$$

where Σ denotes the sum and N is the number of data points.

The size of dominant eddies is characterized by the integral length scale l_t. The horizontal integral length scales can be computed using the autocorrelation of velocity fluctuations (Kundu et al. 2016) as

$$l_{t,x} = U\int_0^{\xi_0} \rho_{uu} d\xi, \quad \rho_{uu}(\xi) = \frac{\overline{u'(t)u'(t+\xi)}}{\overline{u'^2}} \tag{9}$$

in which U is the mean horizontal flow speed, ξ_0 is the first zero-crossing of the autocorrelation function of velocity fluctuations, ξ is the time lag, and ρ_{uu} is the autocorrelation function of the fluctuating velocity component u'.

Results

A new field measurement dataset

The site was sandy with a median grain size of 180 μm and showed no sediment resuspension for the duration of the experiment. Further, the region of interest was also covered with many shells contributing to additional bed roughness. The bed friction factor for the bare-bed region was estimated from the ADCP data as $C_f = 0.0041 \pm 0.00032$ (Fig. 2A) with a p-value < 0.01. The critical velocity and TKE for incipient motion based on the median grain size and bed friction factor were estimated (using Soulsby and Whitehouse 1997) as 0.19 m s^{-1} and 8 $\times 10^{-4}$ m^2 s^{-2}, respectively. These values are greater than those observed for the majority of the observations, so sediment resuspension was expected to be negligible (Fig. 4B,C).

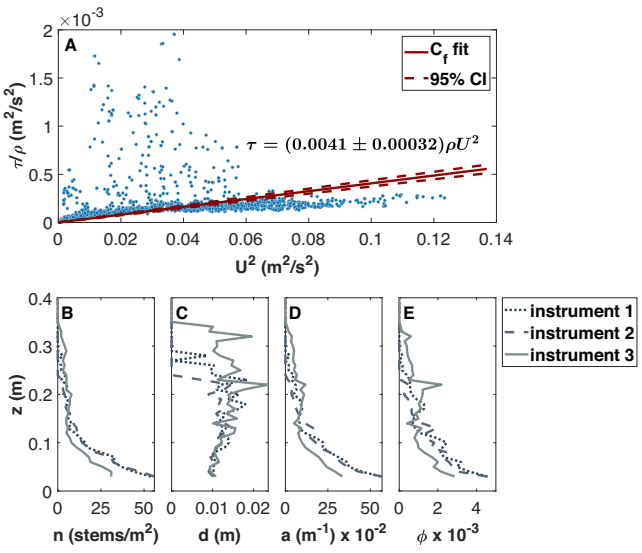

Fig. 2. (**A**) Bare-bed shear stress estimates from the ADCP measurements as a function of the square of depth-averaged flow speed U. Vegetation parameters from underneath the three ADVs determined from the photogrammetric analysis: (**B**) number of stems per square meter, (**C**) mean diameter, (**D**) frontal area per unit volume, (**E**) solid volume fraction.

The pneumatophores were sparsely distributed with a mean height of 100 mm (Fig. 2) within the 1-m^2 quadrats with the profiling ADVs situated at the center of the quadrat. The depth-averaged stem diameters (Fig. 2C) and solid-volume fraction (Fig. 2E) for each quadrat were $d = 10.96$ mm, 10.36 mm, and 10.57 mm, and $\phi = 0.0029$, 0.0026, and 0.0017, respectively. The corresponding frontal areas per bed area for each ADV quadrat were $ah = 0.0339$, 0.0321, and 0.0206 (Fig. 2D). The estimated pneumatophore diameters compare well with the measured values at the field site under each instrument (Supporting Information Fig. S4).

The velocity and pressure data from various instruments (ADVs, ADCPs, and conductivity–temperature–depth sensors) revealed negligible wave activity over the duration of the experiments (Supporting Information Fig. S2). Significant wave heights were estimated from the water–depth time series data from the conductivity–temperature–depth sensor (Supporting Information Fig. S3) for 5-min windows (Green and Coco 2007). Wave heights were predominantly less than 20 mm (98.4% of the record) with maximum values reaching 30 mm. Moreover, times with wave heights of > 20 mm coincided with low signal-to-noise ratios (SNR) values and are discarded during estimating of TKE. Therefore, the data provide a unique set of field data with minimal wave influence for testing the TKE formulations derived under unidirectional flow conditions.

Over the six measured tidal cycles, the maximum water depth was between 0.54 and 0.82 m providing a range of vegetation submergence levels (Fig. 3A). Flow speeds (Fig. 3B) reached a maximum value during the middle of the flood tide, subsequently decreased until the peak water depth was reached, and then increased almost monotonically over the ebb tide. The measured TKE at the three different profile heights using Eq. 5 showed a trend similar to the mean flow speed (Fig. 3C), indicating a correlation between flow speeds and TKE values. Fig. 3D shows that the total TKE generally increased with flow speed, and TKE values from the instruments above the denser quadrats (ADVs 1 and 2) were slightly larger than above the most sparse quadrat (ADV 3).

Evaluation of the vegetation-generated turbulence model

Fig. 4A shows the median value (across all tides and ADVs) of horizontal integral length scales at each water depth $l_{t,x}$ estimated using Eq. 9. For very shallow water depths (<0.15 m), horizontal length scales $l_{t,x}$ are small (<0.1 m), 5–10 times the vegetation typical diameter. Length scales increase substantially as water depths increase, and stabilize to values between 0.1 and 0.17 m for water depths greater than 0.2 m.

The turbulence estimates from the theoretical model are compared against the field measurements. First, the parameter δ of the vegetation-generated turbulence model was obtained by fitting Eq. 7 on aggregated data from all tides and three instruments. Our data yielded a value of the fitting parameter $\delta = 0.52 \pm 0.028$.

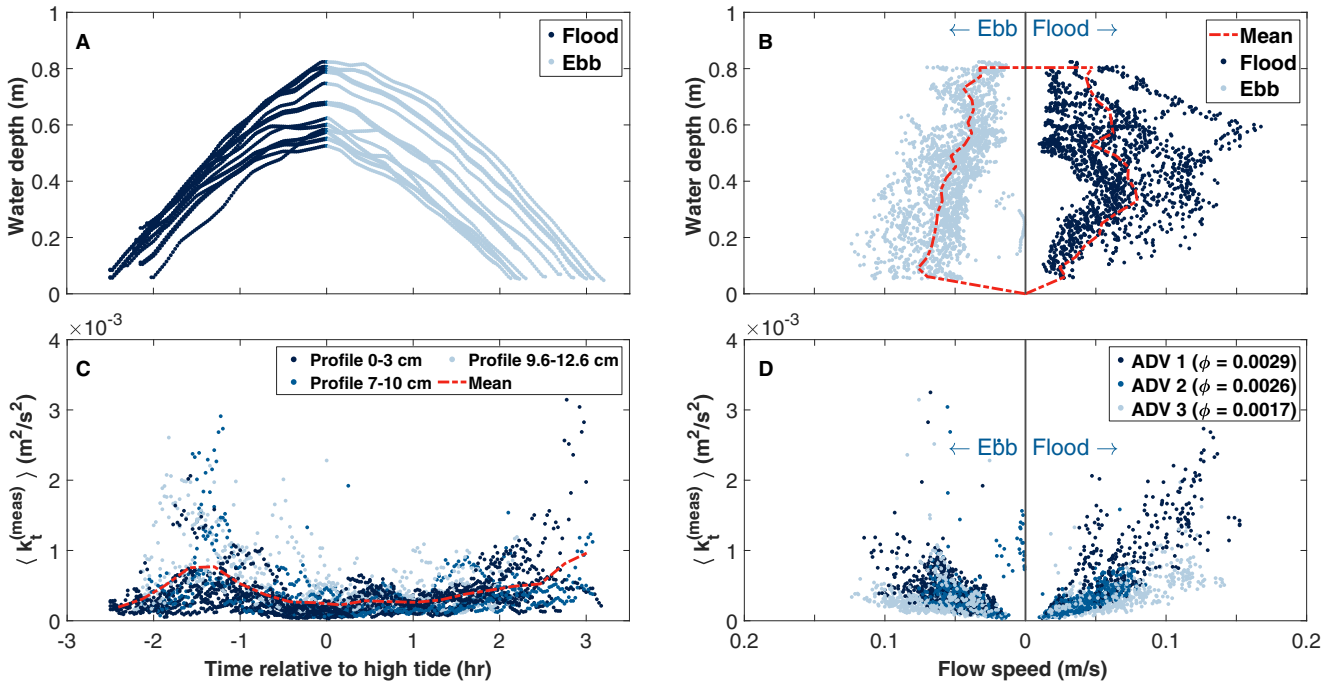

Fig. 3. (**A**) Water depths (dark and light lines show flood and ebb phases of the tide, respectively) plotted against relative time to high tide (defined at the maximum water depth). (**B**) Tidal stage diagram showing water depth vs measured flow speed (dashed line is the mean flow speed). (**C**) Observed TKE (dashed line is the mean observed TKE) plotted against relative time to high tide (defined at the maximum water depth). (**D**) Observed TKE vs. measured flow speed from each ADV.

The performance of the model is shown in Fig. 4B, which shows the predicted and measured TKE (3-min averages). The data from all tides and the three ADVs were combined by sorting into increasing measured TKE values, and then averaged into bins of 100 data points. For TKE values lower than 5×10^{-4} m^2 s^{-2}, the model was in very good agreement within uncertainties, although slightly under-predicts the measured values. However, for larger TKE values, the model under-predicts the observations. The overall MAPE for all the measured TKE values (3-min averages) is 67%. The MAPE observed TKE values over 5×10^{-4} m^2 s^{-2} is 72%, and MAPE for observed TKE values under 1×10^{-4} m^2 s^{-2} is 65%.

Figure 4C shows water depth against flow speed, with points colored by observed vegetation-generated turbulence ($k_{\mathrm{veg}}^{(\mathrm{meas})}$) from Eq. 6. No clear relationship between TKE and water depth can be discerned; however, larger values of $k_{\mathrm{veg}}^{(\mathrm{meas})}$ consistently correspond to faster flow speeds (Fig. 4C). Fig. 4D compares the observed dimensionless vegetation-generated TKE ($\sqrt{k_{\mathrm{veg}}}/U$) values from the field with laboratory observations (Yang and Nepf 2019; Horstman et al. 2018; C. Liu, Shan, et al. 2021; Zhao and Nepf 2021) and theoretical values calculated assuming integral length scales are equal to the stem diameter (dashed line), and assuming integral length scales are equal to 15 times the stem diameter (solid line) as observed in the experiment.

Discussion

Comparison with laboratory experiments

The pneumatophores in the field site were sparse, with smaller volume fractions $\phi = 0.0017 - 0.0029$, than used in laboratory experiments ($\phi = 0.005 - 0.05$), and an order of magnitude sparser than in the majority of previous work (Yang and Nepf 2019; M. Liu, Huai, et al. 2021; Zhao and Nepf 2021). Despite the sparseness of vegetation, the TKE model (Eq. 5) performs reasonably well for low turbulence conditions, with a MAPE between predicted and measured TKE of 62%. The bulk scaling parameter is here computed as $\delta = 0.52 \pm 0.028$, similar to the values found in laboratory experiments by (Zhao and Nepf 2021) ($\delta = 0.52 \pm 0.07$), and (Yang and Nepf 2019) ($\delta = 0.4 \pm 0.3$). The results of this study demonstrate that the TKE model, validated under laboratory channel conditions, can be effectively applied to estimate TKE in real-world field conditions.

One striking difference of the present work is the observed value of integral length-scale l_t. Arguing that the scale of largest eddies is typically the stem diameter, or inter-stem distance when vegetation density is very large, the integral length-scale is usually defined as $l_t = \min\{d, s_n\}$ in which s_n is the average spacing between pneumatophores (Tanino and Nepf 2008; Etminan et al. 2018), with $l_t \sim d$ typically applied. Our observations reveal the length scales can reach up to 15-times the stem diameter (Fig. 4A), indicating that the stem

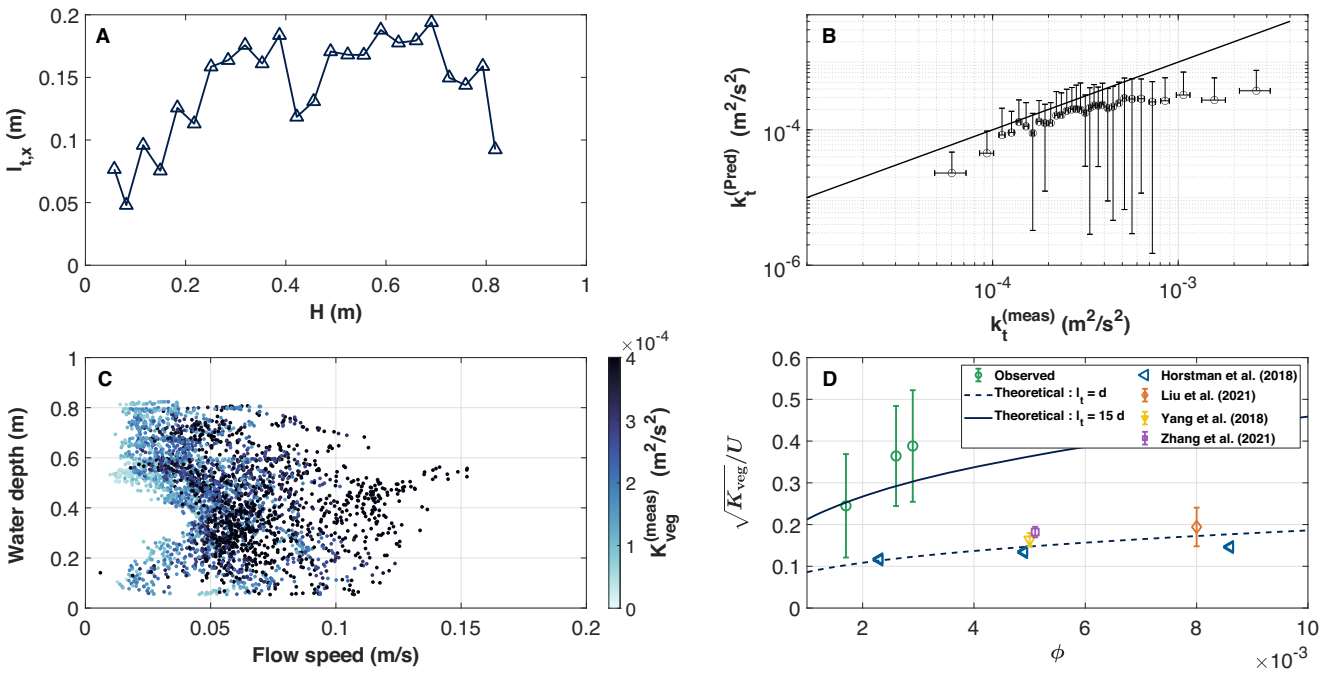

Fig. 4. (**A**) Median horizontal integral length scales $l_{t,x}$ (triangle) estimated from the primary horizontal (u) component of the velocity (9) at different water depths (across all tides and ADVs). (**B**) Predicted TKE estimated using Eq. 4 against measured TKE (5) over all tides sorted by measured values and averaged over bins of 100 points in which the error bars indicate the standard deviation of the values. (**C**) Water depth against flow speed where the points are colored with observed vegetation generated turbulence from Eq. 6. (**D**) Dimensionless vegetation-generated TKE, $\sqrt{k_{veg}}/U$, compared with theoretical values for the current field study and recent laboratory experiments (Yang and Nepf 2019; Horstman et al. 2018; C. Liu, Shan, et al. 2021; Zhao and Nepf 2021). Error bars represent standard deviation.

diameter alone should *not* be used to estimate the turbulent length-scale under real-world conditions with heterogeneous vegetation characterized by multiple length scales.

Necessity of incorporating largest length scales

The value of the integral length-scale indicates turbulence production at scales larger than stem diameter. Since wave activity was absent during the field measurement periods, waves can be excluded as an additional source of turbulence. In addition, *ah* of at least 0.1 is needed for canopy shear layer vortices to appear (Nepf et al. 2007; Nepf 2012b). At the field site, the *ah* value is in the range 0.02 ∓ 0.034. Therefore, shear layer vortices are not expected to be generated by the pneumatophore canopy. The field site is also populated by mangrove saplings of average cross-sectional span of ~ 0.1 m diameter, and ~ 0.2 m height with leaves (Fig. 3B), which is similar to the observed integral length scales at water depths larger than $H > 0.2$ m. At lower water depth, the sapling branches and leaves are emergent, and the integral length scales are closer to the average stem diameter even though it remains larger. This observation suggests that the presence of the saplings, even though very sparse and barely affecting the spatially averaged vegetation characteristics (i.e., the frontal area per unit volume a and volume fraction ϕ), introduces another scale of turbulence, which is advected inside the canopy and towards the measuring instruments.

The spatial heterogeneity of vegetation observed in the field has strong implications in terms of turbulence intensity compared to laboratory conditions (Fig. 4D). Laboratory experiments with real pneumatophore canopies and similar hydrodynamics conditions as in our field experiment (Horstman et al. 2018) found normalized TKE values of $\sqrt{k_t}/U \sim 0.12$ for a pneumatophore canopy of $\phi = 0.005$, water depths of up to 0.3 m (submergence ratios of 1.9–4.7), and for flow speeds of 0.10, and 0.15 m s^{-1} (blue triangles in Fig. 4D). For these similar flow conditions and the slightly lower vegetation densities from the current field site, we find normalized TKE values ($\sqrt{k_t}/U$) between 0.22 and 0.36 on average across the three quadrats (green circles in Fig. 4D), that is, more than twice values recorded in laboratory settings, with the additional turbulence being attributed to production from the nearby saplings. The difference between the laboratory and field conditions is well captured by the vegetation-induced TKE law (Eq. 2) through the dependence on the integral length-scale. Assuming $l_t \sim d$ in Eq. 4, as in laboratory conditions, would lead to severe underestimation of the

vegetation-generated TKE (Fig. 4D) since the measured integral length-scale varies from $l_t \sim 5d$ at low water depth to $l_t \sim 17d$ for $H > 20$ cm (Fig. 4A).

Spatial heterogeneity and sediment transport implications

In order to predict turbulence intensity in natural configurations with heterogeneous vegetation, it is therefore crucial to estimate precisely the integral length-scale, which might be challenging. Our measurements indicate that spatial heterogeneity in vegetation affects the integral length-scale. However, it is not clear from the present results, over which spatial extent it would be necessary to parameterize the spatial heterogeneity. Our measurements revealed similar flow characteristics between the three instruments; which is not surprising instrument locations were similar in terms of distance into the vegetated region and proximity to nearby saplings. Additionally, given the sparsity of the pneumatophores at the field site ($\phi \sim 0.002 - 0.003$), we do not expect the pneumatophores to interact with or significantly attenuate the sapling-generated turbulence. However, for denser root canopies such as in tropical systems, externally generated turbulence would be expected to be either attenuated or transferred from sapling to stem scale through the spectral shortcut mechanism (Finnigan 2000). The assumption of $l_t \sim d$ would still apply and the interior of the canopy would be isolated from the turbulence generated outside.

One of the main motivations for developing TKE prediction models is to predict sediment transport. In the presence of vegetation, it has been observed that TKE is a reliable predictor of incipient motion (Yang et al. 2016; Tinoco and Coco 2018), sediment transport (Yang and Nepf 2018, 2019) and resuspension (Tinoco and Coco 2014; Xu and Nepf 2020). Recent approaches in formulating bedload transport in vegetated flows have adapted τ-based formulations to k_t-based formulations. Therefore, the vegetation-generated TKE law could be implemented in numerical models (e.g., depth-averaged models) to predict sediment transport, providing a significant change for large-scale modeling of coastal geomorphic evolution. The results of the present study suggest that current laboratory-derived formulations can be used to predict of the efficacy of aquatic vegetation as a nature-based solution for protection against coastal hazards, so long as the existence of multiple vegetation length scales are considered and parameterized appropriately.

Author Contributions

Julia C. Mullarney, Vinay Nelli, and Rémi Chassagne designed research. Julia C. Mullarney, Vinay Nelli, and Rémi Chassagne undertook field experiments. Vinay Nelli analyzed data. All authors interpreted results and contributed to paper writing. Julia C. Mullarney, Rafael O. Tinoco, William Nardin acquired funding.

Acknowledgments

This research is funded by the Royal Society of New Zealand's Marsden Fund (Grant Number 20-UOW-030). We thank Ben Roche for helping with the field experiments. We thank two anonymous reviewers and the editors for their comments which helped to improve the manuscript.

Data Availability Statement

Data are available on the Figshare repository https://doi.org/10.6084/m9.figshare.30142627.v2.

References

Anjum, N., and N. Tanaka. 2020. "Investigating the Turbulent Flow Behaviour Through Partially Distributed Discontinuous Rigid Vegetation in an Open Channel." *River Research and Applications* 36, no. 8: 1701–1716. https://doi.org/10.1002/rra.3671.

Barbier, E. B., S. D. Hacker, C. Kennedy, E. W. Koch, A. C. Stier, and B. R. Silliman. 2011. "The Value of Estuarine and Coastal Ecosystem Services." *Ecological Monographs* 81, no. 2: 169–193. https://doi.org/10.1890/10-1510.1.

Biron, P. M., C. Robson, M. F. Lapointe, and S. J. Gaskin. 2004. "Comparing Different Methods of Bed Shear Stress Estimates in Simple and Complex Flow Fields." *Earth Surface Processes and Landforms* 29, no. 11: 1403–1415. https://doi.org/10.1002/esp.1111.

Chen, M., S. Lou, S. Liu, et al. 2020. "Velocity and Turbulence Affected by Submerged Rigid Vegetation Under Waves, Currents and Combined Wave–Current Flows." *Coastal Engineering* 159: 103727. https://doi.org/10.1016/j.coastaleng.2020.103727.

Conde-Frias, M., M. Ghisalberti, R. J. Lowe, M. Abdolahpour, and V. Etminan. 2023. "The Near-Bed Flow Structure and Bed Shear Stresses Within Emergent Vegetation." *Water Resources Research* 59, no. 4: e2022WR032499. https://doi.org/10.1029/2022WR032499.

Costanza, R., R. d'Arge, R. de Groot, et al. 1997. "The Value of the World's Ecosystem Services and Natural Capital." *Nature* 387, no. 6630: 253–260. https://doi.org/10.1038/387253a0.

Etminan, V., M. Ghisalberti, and R. J. Lowe. 2018. "Predicting Bed Shear Stresses in Vegetated Channels." *Water Resources Research* 54, no. 11: 9187–9206. https://doi.org/10.1029/2018WR022811.

Finnigan, J. 2000. "Turbulence in Plant Canopies." *Annual Review of Fluid Mechanics* 32, no. 1: 519–571. https://doi.org/10.1146/annurev.fluid.32.1.519.

Goring, D. G., and V. I. Nikora. 2002. "Despiking Acoustic Doppler Velocimeter Data." *Journal of Hydraulic Engineering* 128, no. 1: 117–126. https://doi.org/10.1061/(ASCE)0733-9429(2002)128:1(117).

Green, M. O., and G. Coco. 2007. "Sediment Transport on an Estuarine Intertidal Flat: Measurements and Conceptual

Model of Waves, Rainfall and Exchanges With a Tidal Creek." *Estuarine, Coastal and Shelf Science* 72, no. 4: 553–569. https://doi.org/10.1016/j.ecss.2006.11.006.

Horstman, E. M., K. R. Bryan, J. C. Mullarney, C. A. Pilditch, and C. A. Eager. 2018. "Are Flow-Vegetation Interactions Well Represented by Mimics? A Case Study of Mangrove Pneumatophores." *Advances in Water Resources* 111: 360–371. https://doi.org/10.1016/j.advwatres.2017.11.018.

Hu, Z., S. Temmerman, Q. Zhu, et al. 2025. "Predicting Nature-Based Coastal Protection by Mangroves Under Extreme Waves." *Proceedings of the National Academy of Sciences of the United States of America* 122, no. 12: e2410883122. https://doi.org/10.1073/pnas.2410883122.

Kim, S.-C., C. T. Friedrichs, J. P.-Y. Maa, and L. D. Wright. 2000. "Estimating Bottom Stress in Tidal Boundary Layer From Acoustic Doppler Velocimeter Data." *Journal of Hydraulic Engineering* 126, no. 6: 399–406. https://doi.org/10.1061/(ASCE)0733-9429(2000)126:6(399).

King, A. T., R. O. Tinoco, and E. A. Cowen. 2012. "A *k*-ε Turbulence Model Based on the Scales of Vertical Shear and Stem Wakes Valid for Emergent and Submerged Vegetated Flows." *Journal of Fluid Mechanics* 701: 1–39. https://doi.org/10.1017/jfm.2012.113.

Kundu, P. K., I. M. Cohen, D. R. Dowling, and G. Tryggvason. 2016. *Fluid Mechanics*. 6th ed. Elsevier/AP.

Liénard, J., K. Lynn, N. Strigul, et al. 2016. "Efficient Three-Dimensional Reconstruction of Aquatic Vegetation Geometry: Estimating Morphological Parameters Influencing Hydrodynamic Drag." *Estuarine, Coastal and Shelf Science* 178: 77–85. https://doi.org/10.1016/j.ecss.2016.05.011.

Liu, C., Y. Shan, and H. Nepf. 2021. "Impact of Stem Size on Turbulence and Sediment Resuspension Under Unidirectional Flow." *Water Resources Research* 57, no. 3: e2020WR028620. https://doi.org/10.1029/2020WR028620.

Liu, M., W. Huai, and B. Ji. 2021. "Characteristics of the Flow Structures Through and Around a Submerged Canopy Patch." *Physics of Fluids* 33, no. 3: 035144. https://doi.org/10.1063/5.0041782.

Montgomery, J. M., K. R. Bryan, J. C. Mullarney, and E. M. Horstman. 2019. "Attenuation of Storm Surges by Coastal Mangroves." *Geophysical Research Letters* 46, no. 5: 2680–2689. https://doi.org/10.1029/2018GL081636.

Nepf, H. M. 2012*a*. "Flow and Transport in Regions With Aquatic Vegetation." *Annual Review of Fluid Mechanics* 44, no. 1: 123–142. https://doi.org/10.1146/annurev-fluid-120710-101048.

Nepf, H. M. 2012*b*. "Hydrodynamics of Vegetated Channels." *Journal of Hydraulic Research* 50, no. 3: 262–279. https://doi.org/10.1080/00221686.2012.696559.

Nepf, H. M., M. Ghisalberti, B. White, and E. Murphy. 2007. "Retention Time and Dispersion Associated With Submerged Aquatic Canopies." *Water Resources Research* 43, no. 4: W04422. https://doi.org/10.1029/2006WR005362.

Norris, B. K., J. C. Mullarney, K. R. Bryan, and S. M. Henderson. 2019. "Turbulence Within Natural Mangrove Pneumatophore Canopies." *Journal of Geophysical Research: Oceans* 124, no. 4: 2263–2288. https://doi.org/10.1029/2018JC014562.

Norris, B. K., J. C. Mullarney, K. R. Bryan, and S. M. Henderson. 2021. "Relating Millimeter-Scale Turbulence to Meter-Scale Subtidal Erosion and Accretion across the Fringe of a Coastal Mangrove Forest." *Earth Surface Processes and Landforms* 46, no. 3: 573–592. https://doi.org/10.1002/esp.5047.

Pollen, N., and A. Simon. 2005. "Estimating the Mechanical Effects of Riparian Vegetation on Stream Bank Stability Using a Fiber Bundle Model." *Water Resources Research* 41, no. 7: 2004WR003801. https://doi.org/10.1029/2004WR003801.

Schlichting, H. 1979. "Boundary-Layer Theory. Engger." In *McGraw-Hill Series in Mechanical Engineering*, 7th ed. New York: McGraw-Hill.

Soulsby, R. L. 1983. "Chapter 5: The Bottom Boundary Layer of Shelf Seas." In *Elsevier Oceanography Series*, vol. 35, 189–266. Elsevier. https://doi.org/10.1016/S0422-9894(08)70503-8.

Soulsby, R. L., and R. J. S. Whitehouse. 1997. *Pacific Coasts and Ports '97: Proceedings of the 13th Australasian Coastal and Ocean Engineering Conference and the 6th Australasian Port and Harbour Conference; Volume 1*. Christchurch, N.Z: Centre for Advanced Engineering, University of Canterbury.

Tanino, Y., and H. M. Nepf. 2008. "Lateral Dispersion in Random Cylinder Arrays at High Reynolds Number." *Journal of Fluid Mechanics* 600: 339–371. https://doi.org/10.1017/S0022112008000505.

Temmerman, S., E. M. Horstman, K. W. Krauss, J. C. Mullarney, I. Pelckmans, and K. Schoutens. 2023. "Marshes and Mangroves as Nature-Based Coastal Storm Buffers." *Annual Review of Marine Science* 15, no. 1: 95–118. https://doi.org/10.1146/annurev-marine-040422-092951.

Tinoco, R. O., and G. Coco. 2014. "Observations of the Effect of Emergent Vegetation on Sediment Resuspension Under Unidirectional Currents and Waves." *Earth Surface Dynamics* 2, no. 1: 83–96. https://doi.org/10.5194/esurf-2-83-2014.

Tinoco, R. O., and G. Coco. 2018. "Turbulence as the Main Driver of Resuspension in Oscillatory Flow Through Vegetation." *Journal of Geophysical Research. Earth Surface* 123, no. 5: 891–904. https://doi.org/10.1002/2017JF004504.

Tinoco, R. O., J. E. San Juan, and J. C. Mullarney. 2020. "Simplification Bias: Lessons From Laboratory and Field Experiments on Flow Through Aquatic Vegetation." *Earth Surface Processes and Landforms* 45, no. 1: 121–143. https://doi.org/10.1002/esp.4743.

van Katwijk, M. M., A. Thorhaug, N. Marbà, et al. 2016. "Global Analysis of Seagrass Restoration: The Importance

of Large-Scale Planting." *Journal of Applied Ecology* 53, no. 2: 567–578. https://doi.org/10.1111/1365-2664.12562.

Vettori, D., F. Giordana, and C. Manes. 2025. "Turbulence Enhances Wave Attenuation of Seagrass in Combined Wave–Current Flows." *Proceedings of the National Academy of Sciences of the United States of America* 122, no. 6: e2414150122. https://doi.org/10.1073/pnas.2414150122.

Williams, J. J. 1995. "Drag and Sediment Dispersion Over Sand Waves." *Estuarine, Coastal and Shelf Science* 41, no. 6: 659–687. https://doi.org/10.1006/ecss.1995.0083.

Xu, Y., and H. Nepf. 2020. "Measured and Predicted Turbulent Kinetic Energy in Flow Through Emergent Vegetation With Real Plant Morphology." *Water Resources Research* 56, no. 12: e2020WR027892. https://doi.org/10.1029/2020WR027892.

Yager, E. M., and M. W. Schmeeckle. 2013. "The Influence of Vegetation on Turbulence and Bed Load Transport." *Journal of Geophysical Research: Earth Surface* 118, no. 3: 1585–1601. https://doi.org/10.1002/jgrf.20085.

Yang, J. Q., and H. M. Nepf. 2018. "A Turbulence-Based Bed-Load Transport Model for Bare and Vegetated Channels." *Geophysical Research Letters* 45, no. 19: 10,428–10,436. https://doi.org/10.1029/2018GL079319.

Yang, J. Q., and H. M. Nepf. 2019. "Impact of Vegetation on Bed Load Transport Rate and Bedform Characteristics." *Water Resources Research* 55, no. 7: 6109–6124. https://doi.org/10.1029/2018WR024404.

Yang, J. Q., F. Kerger, and H. M. Nepf. 2015. "Estimation of the Bed Shear Stress in Vegetated and Bare Channels With Smooth Beds." *Water Resources Research* 51, no. 5: 3647–3663. https://doi.org/10.1002/2014WR016042.

Yang, J. Q., H. Chung, and H. M. Nepf. 2016. "The Onset of Sediment Transport in Vegetated Channels Predicted by Turbulent Kinetic Energy." *Geophysical Research Letters* 43, no. 21: 11,261–11,268. https://doi.org/10.1002/2016GL071092.

Zhao, T., and H. M. Nepf. 2021. "Turbulence Dictates Bedload Transport in Vegetated Channels Without Dependence on Stem Diameter and Arrangement." *Geophysical Research Letters* 48, no. 21: e2021GL095316. https://doi.org/10.1029/2021GL095316.

Supporting Information

Additional Supporting Information may be found in the online version of this article.

Submitted 17 September 2025
Revised 29 November 2025
Accepted 19 December 2025